Effects of IIIB transition metals on optoelectronic and magnetic properties of $HoMnO_3$: A first principles study

H. A. Rahnamaye Aliabad[a)†] and Battal G. Yalcin[b)]

[a)] Department of Physics, Hakim Sabzevari University, Sabzevar, Iran
[b)] Department of Physics, Sakarya University, Serdivan, Sakarya, Turkey

(Received 8 May 2015; revised manuscript received 10 July 2015; published online 9 October 2015)

The optoelectronic and magnetic properties of pure $HoMnO_3$ and $Ho_{0.67}T_{0.33}MnO_3$ (T = La, Y) alloys in hexagonal phase are theoretically investigated by using the first-principles calculations. The investigations are performed by means of the density functional theory through using the spin polarized generalized gradient approximation plus the Hubbard potential (SPGGA + U, $U_{\rm eff} = 3$ eV). The studied material $HoMnO_3$ exhibits two indirect band gaps: 1.58 eV for the spin-up state and 0.72 eV for the spin-down state along the S–G direction within the SPGGA + U approximation. It is found that the band gap of pure $HoMnO_3$ for the spin-up state increases with increasing La and Y dopants. The results show that all of the studied materials have semi-metallic behaviors for the spin-up state and semiconducting character for the spin-down state. The substitutions of La and Y for Ho in $HoMnO_3$ cause the static dielectric constant (ε_0) to increase in the x direction but to decrease in the z direction. The calculated optical conductivity spectrum of $HoMnO_3$ in a low energy range is in good agreement with the recent experimental data.

Keywords: optoelectronic and magnetic properties, $HoMnO_3$, Hubbard potential

PACS: 71.15.Mb, 75.25.–j, 78.20.Ci **DOI:** 10.1088/1674-1056/24/11/117102

1. Introduction

Occurrences of the magnetic and ferroelectric orders in $HoMnO_3$ are the main reasons for investigating the electronic, optical, and magnetic properties of this compound.[1] Moreover, the passion for studying the magneto–electronic interaction mechanism has also induced scientists to make their efforts to explore this system as a material in new spintronic devices.[2] It is fascinating to note that we can use the coupling effects for new types of devices in microelectronic and digital memory applications;[3] they are indeed limber frameworks for developing novel functional materials.[4] Anomalies in the dielectric constants, the linear expansion coefficients, and the phonon frequencies suggest coupling between the magnetic and the ferroelectric orders at low temperatures in these systems.[5]

The rare earth manganites or ferroelectrics like RMnO$_3$, RMn$_2$O$_5$, and R_2Mn$_2$O$_7$ (R = rare earth) compounds are a group of the perovskite families with interesting properties that exhibit both magnetic order and ferroelectricity[3] in the same phase.[2] The RMnO$_3$ systems are crystallized in hexagonal (with $P6_3cm$ space group) and orthorhombic (with $P6_3mmc$ space group) structures.[6] Crystallizing of the rare-earth manganites in the two kinds of structures relies on the ionic radius of the R atom. The RMnO$_3$ manganites with smaller ionic radii (R = Sc, Y, Ho, Er, Tm, Yb, Lu) are in the hexagonal structure.[2] The hexagonal manganites are ferroelectric at high temperatures (over $T_{\rm c} \approx 900$ K)[7] and can be stabilized in large radius cation systems.[8] Gao *et al.* showed that the increase of the pressure induces a transition from hexagonal to orthorhombic phase in structure.[6] Their measurements of x-ray diffraction on magnetic multiferroic hexagonal RMnO$_3$ (R = Y, Ho, Lu) verified that the hexagonal structure is stable below ~ 20 GPa. The results obtained by Makhnev *et al.* showed that hexagonal RMnO$_3$ is a charge-transfer insulator.[2]

$HoMnO_3$ is a member of the RMnO$_3$ family, and its hexagonal and orthorhombic structures have been extensively studied. The antiferromagnetic behavior of $HoMnO_3$ is observed below $T_{\rm N} = 75$ K.[4] In zero field, Ho^{+3} orders antiferromagnetically with the moments aligned along the hexagonal c direction, and the magnetic structure of Ho^{+3} remains unchanged in applied electric fields up to 1×10^7 V/m below 40 K.[9] An unusual antiferroelectric-like behavior is also observed above 40 K.[10] In the $YMnO_3$ compound with $P6_3cm$ space group, the ferroelectricity properties are observed at 800 K. Lonkai *et al.* reported that $HoMnO_3$ and $YMnO_3$ compounds are isomorphic materials.[1]

In this paper, we investigate the optoelectronic and magnetic properties of pure $HoMnO_3$ and $Ho_{0.67}T_{0.33}MnO_3$ (T = La, Y) alloys. There are two symmetric positions for the Ho element (Ho_1 and Ho_2). In comparison with the Ho_2 site, the Ho_1 site has a higher symmetry and is more stable; therefore we substitute La and Y to the Ho_1 site as shown in Fig. 1. We use the hexagonal structure with space group $P6_3cm$ (space group No. 185) in the ferroelectric state. In this structure, one Mn atom and five adjacent oxygen atoms form

†Corresponding author. E-mail: Rahnama@hsu.ac.ir

© 2015 Chinese Physical Society and IOP Publishing Ltd

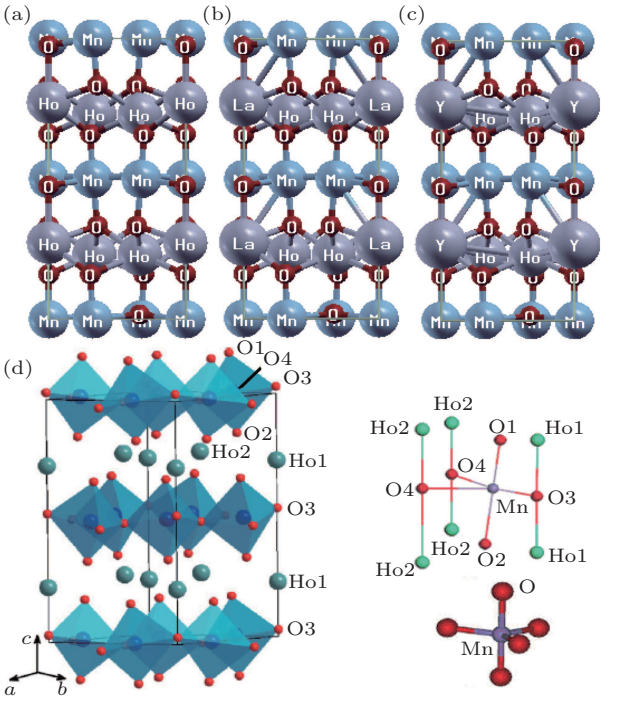


Fig. 1. (color online) Crystal structures of (a) $HoMnO_3$, (b) $Ho_{0.67}La_{0.33}MnO_3$, (c) $Ho_{0.67}La_{0.33}MnO_3$, and (d) $HoMnO_3$ cited from Ref. [4].

a MnO_5 trigonal bipyramid. It is worthwhile noticing that in view of symmetry, there are two nonequivalent Ho atoms, four nonequivalent O atoms, and one Mn atom in the unit cell of the system. We use the experimental lattice constant and then find theoretically the lattice constants by optimizing the total energy with respect to the unit cell volume of the crystal. Our obtained structural properties of the pure $HoMnO_3$ and $Ho_{0.67}T_{0.33}MnO_3$ (T = La, Y) compounds are presented in Table 1.

The rest of this article is organized as follows. We provide the technical details of calculations in Section 2. Our results are given in Sections 3–6. Some conclusions are drawn in Section 7.

2. Computational details

The full potential linearized augmented plane wave (FP-LAPW) method based on the density functional theory is used for the optoelectronic calculations with the Wien2k code.[11] For calculating the exchange–correlation potential, the spin polarized generalized gradient approximation plus the

Table 1. Obtained structural, electrical, magnetic, and optical data for $Ho_{1-x}T_xMnO_3$ ($x = 0$, 0.33; T = La, Y) together with results of the others for comparison.

Properties	Present work			Others
	$HoMnO_3$	$Ho_{0.67}La_{0.33}MnO_3$	$Ho_{0.67}Y_{0.33}MnO_3$	$HoMnO_3$
$a = b$	6.14	6.15	6.10	6.12 [a]
c	11.45	11.49	11.56	11.41[a]
R_{MT}(Ho)	2.27	2.28	2.27	
R_{MT}(Mn)	1.83	1.97	1.97	
R_{MT}(O)	1.62	1.50	1.53	
R_{MT}(La)	–	2.27	–	
R_{MT}(Y)	–	–	2.26	
SPGGA:				
$E_{g,up}$/eV	1.67	1.86	1.83	1.5[b], 1.7[a]
Magnetic moments:				
M_{Ho1}	3.92	–	–	3.12[c]
M_{La}	–	0.02	–	–
M_Y	–	–	0.02	–
M_{Ho2}	3.90	3.92	3.92	–
M_{Mn}	3.31	3.46	3.47	3.51[c]
M_{int}	3.37	2.53	2.53	–
M_{Cell}	47.79	40.01	40.03	–
$\varepsilon_1(\omega)$:				
ε_0^x	23.38	29.56	29.96	–
ε_0^z	6.69	6.50	6.31	–
ε^x(1.6 eV)	3.84	3.92	3.85	4.1[d]
SPGGA + U:				
$E_{g,up}$/eV	1.58	1.82	1.67	1.5[b], 1.7[a]
Magnetic moments:				
M_{Ho1}	3.90	–	–	3.12[c]
M_{La}	–	0.01	–	–
M_Y	–	–	0.01	–
M_{Ho2}	3.90	3.90	3.90	–
M_{Mn}	3.46	3.61	3.48	3.51[c]
M_{int}	3.18	2.20	2.96	–
M_{Cell}	48.00	39.96	40.01	–
$\varepsilon_1(\omega)$:				
ε_0^x	16.04	18.02	16.66	–
ε_0^z	5.75	5.79	5.66	–
ε^x(1.6 eV)	3.90	4.18	3.79	4.1[d]

[a] Ref. [18], Exp.; [b] Ref. [2], Exp.; [c] Ref. [1], Exp.; [d] Ref. [4], Exp.

Hubbard potential (SPGGA + U)[12,13] is used. Selected muffin-tin radii are given in Table 1. For the optoelectronic calculations, we use a dense k-mesh, leading to 1000 k-points in the irreducible first Brillouin zone. In the calculations, the diagonal density matrix U[14,15] is identical for all Coulomb and exchange interactions and we use the self-interaction correction (SIC) as implemented in the Wien2k code. There are several methods for calculating $U_{\rm eff}$.[16,17] The results of the density of states (DOS) within the SPGGA ($U_{\rm eff} = 0$ eV) show that the Mn 3d state is located at lower binding energies compared with the experimental results, as shown in Fig. 2. We can shift the position of the Mn 3d state toward larger binding energies with increasing $U_{\rm eff}$. By adjusting the first main peak of the Mn 3d state to the experimental value about 1.7 eV,[4] the effective Hubbard parameter $U_{\rm eff} = 3$ eV is obtained.

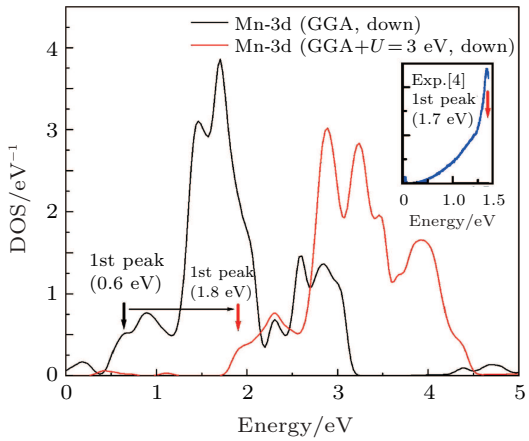


Fig. 2. (color online) Mn 3d partial DOSs calculated by using GGA and GGA + U ($U = 3$ eV).

3. Band structure and density of states

The physical properties of compounds are directly or indirectly related to the electronic band structures. The band structures of the studied materials are calculated along the high symmetry directions in the primitive Brillouin zone (Fig. 3), and the results are shown in Fig. 4. The Fermi levels in all the plots are all shifted to zero on the energy scale. The band gaps of all considered structures are presented in Table 1 for the spin up states. The obtained indirect band gaps for $HoMnO_3$ are $1.67^{\rm SPGGA}$ eV and $1.58^{\rm SPGGA+U}$ eV ($0.62^{\rm SPGGA}$ eV and $0.72^{\rm SPGGA+U}$ eV) for the spin up (down) states in the $S \rightarrow G$ direction. Our results are in close agreement with the experimental values (1.5 eV[2] and 1.7 eV[18]). The results show that all of the studied materials have semi-metallic behaviors for the spin-up states due to the electronic bands crossing the Fermi level and semiconducting character for the spin-down states. As shown in Fig. 4, for the spin-up states, the band gap of the material appears on the top of the Fermi level from 1.7 eV to 3.6 eV. Substitutions of La and Y for Ho in $HoMnO_3$ cause the band gaps in SPGGA and SPGGA + U to increase.

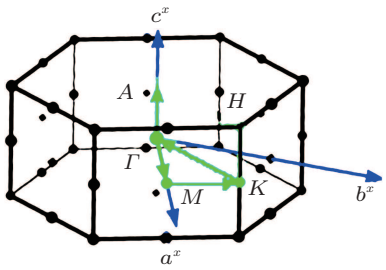


Fig. 3. (color online) Selected directions in the primitive Brillouin zone.

The analysis of the partial DOS of $HoMnO_3$ reveals the most contribution of each atom in each distinct energy category. Figure 5 shows the total DOSs of pure $HoMnO_3$ and the $HoMnO_3$ doped with La, Y for the spin-up and spin-down states. For pure $HoMnO_3$, the Ho-5p state combined with a negligible share of the O-1s state dominates the energy range from −25 eV to −23 eV in the SPGGA + U calculation. The peaks between −19 eV to −20 eV originate from the O-2s states with minimum contribution of the Ho-5p state, and the peaks between −19 eV to −18 eV result from O-2s with some contribution of the Ho-5p state. The peak around −17 eV is also derived from O-2s. Finally, the fifth group from −7 eV to −1.5 eV is due to the O-2p, Mn-3d, and Ho-4f states. In this range, the O-2p state shows dominancy while the contributions of the O-2p and Mn-3d states are moderate and the contribution of Ho-5p is minimal. We note that the Ho-4f, Mn-3d, and O-2p states are strongly hybridized, leading to the covalent bond between Ho–O and Mn–O, which is in good agreement with the previous results.[18] As can be seen in Fig. 5, the sizeable proportion of the valence bands are constituted on the Fermi level which originate mostly from the Mn-3d state mixed with the minimal allocation of the O-2p state. However, the next group of states in an energy range from 3 eV to 12 eV are generated by the combination of the Ho-4d and O-2p states.

The calculated DOS for $Ho_{0.67}La_{0.33}MnO_3$ by SPGGA + U shows that partial DOS of La is predominately introduced into the conduction bands at 6.0–7.5 eV. Compared with those of pure $HoMnO_3$, in this case, the DOSs, especially the valence bands around the Fermi level and the lowest conduction bands, are shifted toward the higher energies. The partial DOS of $Ho_{0.67}La_{0.33}MnO_3$ shows a small proportion of La-5p state in a range from −20 eV to −15 eV. The surplus peaks in the range from −15 eV to −10 eV originate from the La-5p state combined with a negligible share of O 2p and 2s states. The conduction band in the range from 3 eV to 12 eV is composed of the La-4f state hybridized with a noticeable share of Ho-4d and La-5d states and negligible O-2p state.

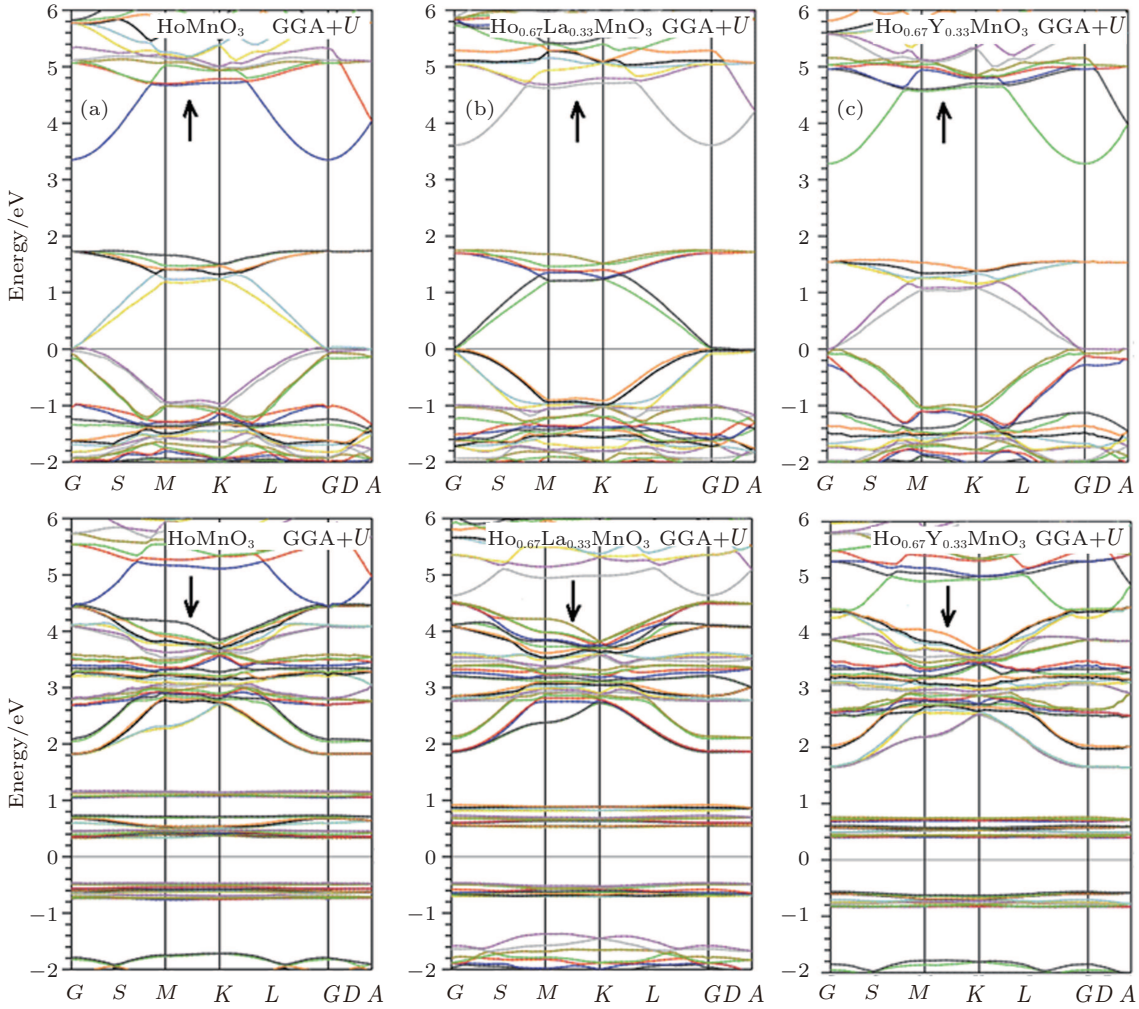


Fig. 4. (color online) Band structures for $Ho_{1-x}T_x$ MnO_3: (a) $x = 0$; (b) $x = 0.33$, T = La; (c) $x = 0.33$, T = Y.

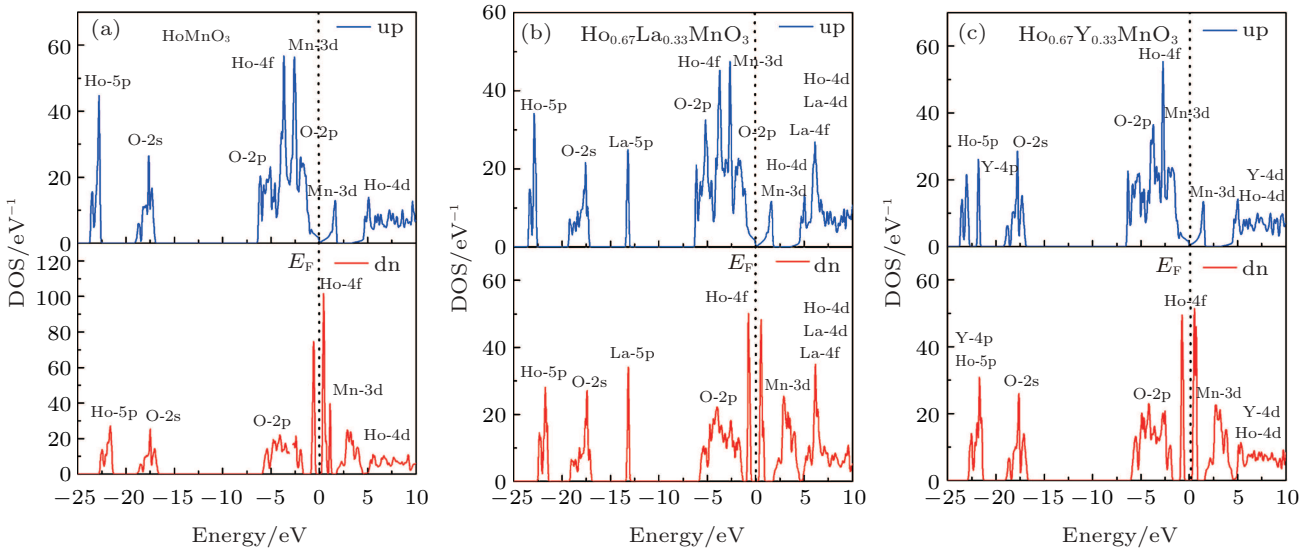


Fig. 5. (color online) DOSs for (a) $HoMnO_3$, (b) $Ho_{0.67}La_{0.33}MnO_3$, and (c) $Ho_{0.67}Y_{0.33}MnO_3$ obtained by using SPGGA + U.

For the spin-up and the spin-down states, the critical differences between them result from the Ho-4f and Mn-3d states. The results show that in the spin down states, the Ho-4f state is more separated from the Mn-3d state. For all materials at the spin up states, there is a weak hybridization between the Ho-5p and O-2s states in the range from −20 eV to −15 eV. In this case, we can see a strong combination between the Ho-4f and O-2p states just under the Fermi level and a strong mixture

between the Mn-3d and O-2p states[19] just under and over the Fermi level. Also, there is a slight blend between the Ho-4d and O-2p states in the conduction band, higher than 3 eV. The Mn-3d state above the Fermi level is separated from the Ho-4f state in the SPGGA + U schema. In the $Ho_{0.67}Y_{0.33}MnO_3$ compound, for the spin-up states, the Y-4p states appear in the range from −25 eV to −20 eV and the Y-4d states contribute to Ho-4d in the conduction band. Finally, for the spin-down states, the Y-4p state cooperates with the Ho-5p state in the range from −25 eV to −20 eV.

4. Spin magnetic moments

The Mn layers play an important role in determining the magnetic properties of $HoMnO_3$ along the c direction.[20–22] It is predicated that the substitutions of La and Y atoms change the c parameter and, as a result, change the magnetic properties. The net magnetic moments of $Ho_{1-x}T_xMnO_3$ ($x = 0$, 0.33; T = La, Y) are due to the contributions of the magnetic moments of Ho_1, Ho_2, Mn, and interstitial sites as presented in Table 1. Most of the contributions come from the unfilled Ho_1-4f, Ho_2-4f, Mn-3d states and the interstitial sites. The results show that the magnetic moment at the Mn site increases by adding La and Y atoms. This increase is due to the decrease in the bonding strength with the increase in the c parameter of the unit cell. This increase in the magnetization at the Mn site spontaneously induces the magnetic moments at the non-magnetic sites. The net magnetic moment of the unit cell decreases because of the substitutions of non-magnetic atoms (La and Y) for the magnetic atoms (Ho).

5. Dielectric function

Transitions between occupied and unoccupied states occur in the electric field of the photon, including plasmons and single particle excitations. The linear response of a system to an electromagnetic radiation is described by the dielectric function $\varepsilon(\omega)$.[23] For calculating the frequency dependent dielectric function $\varepsilon(\omega)$, we need energy eigenvalues and electron wave functions. Both energy eigenvalues and electron wave functions are the natural outcomes of the band structure calculations. The symmetry of the reported crystal structure implies that there are two non-zero components for the dielectric tensor along $a = b$ and c crystallographic axes. The two principal complex tensor components for the single crystal are $\varepsilon^{xx}(\omega)$ and $\varepsilon^{zz}(\omega)$. We need to calculate the two components of the imaginary part of the dielectric function for a complete characterization of the linear optical properties. In the random phase approximation (RPA) as implemented in the WIEN2k code, we use the following equations for calculating the complex dielectric tensor:[24]

$$\mathrm{Im}\varepsilon_{\alpha\beta}^{\{\mathrm{inter}\}}(\omega) = \frac{\hbar^2 e^2}{\pi m^2 \omega^2} \sum_{c,v} \int \mathrm{d}k \langle c_k | p^\alpha | v_k \rangle \langle v_k | p^\beta | c_k \rangle \times \delta(\varepsilon_{ck} - \varepsilon_{vk} - \omega), \quad (1)$$

$$\mathrm{Re}\varepsilon_{\alpha\beta}(\omega) = \delta_{\alpha\beta} + \frac{2}{\pi} \mathrm{P} \int_0^\infty \frac{\omega' \mathrm{Im}\varepsilon_{\alpha\beta}(\omega')}{\omega'^2 - \omega^2} \mathrm{d}\omega', \quad (2)$$

where P denotes the principle value of the integral. The real parts of the frequency dependent dielectric function for $Ho_{1-x}T_xMnO_3$ ($x = 0$, 0.33; T = La, Y) are shown in Fig. 6 for the x and z directions. The square of the dielectric function in zero energy is equal to the static refractive index. The obtained static refractive index for $HoMnO_3$ is very large 4.83 in the plane perpendicular to the c axis (x and y directions), while it is 2.59 in the plane parallel to the c axis (z direction) within the SPGGA schema. This property is called birefringence and it is observed in optically anisotropic materials. The substitutions of La and Y for Ho in $HoMnO_3$ cause ε_0^{xx} (or n_0^{xx}) to increase within both SPGGA and SPGGA + U approximations. Figure 6 shows that $\varepsilon_1(\omega)$ is zero at certain energies and then decreases to negative values. The real part of the dielectric function is zero at the plasmon frequency (ω_p), and the negative dielectric function means that the incident electromagnetic waves are totally reflected and hence the material exhibits a strong metallic character. The negative values of $\varepsilon_1(\omega)$ also correspond to the local maxima of absorption or reflectivity.

Roots of the dielectric function ($\varepsilon(\omega_\mathrm{p}) = 0$) are necessary factors to stimulate the oscillations of plasmons. In SPGGA + U, the roots of $\varepsilon_1(\omega)$ are located at higher energies compared to those in SPGGA. Moreover, the number of roots increases from 6 to 10 for $Ho_{0.67}La_{0.33}MnO_3$ in the z direction. These behaviors are observed for $Ho_{0.67}Y_{0.33}MnO_3$ in the x direction for both approximations. There are more roots along the z direction than along the x direction for both $Ho_{0.67}La_{0.33}MnO_3$ and $Ho_{0.67}Y_{0.33}MnO_3$.

The imaginary part of the dielectric function, $\varepsilon_2^{\mathrm{average}}(\omega)$, can be divided into direct and indirect band transitions. The electric dipole transitions between occupied and unoccupied bands are generally used to determine the peaks in the optical response. These peaks can be identified by using the band structure or the total DOS. The peaks in the calculated spectra of ε_2 display the transition of electrons from occupied (VB) to unoccupied bands (CB). The imaginary parts of the frequency dependent dielectric function for $Ho_{1-x}T_xMnO_3$ ($x = 0$, 0.33; T = La, Y) are shown in Fig. 7 for x and z components. The peaks on the $\varepsilon_2(\omega)$ curves (E_0, E_1, E_2, E_3) are related to the interband transitions from the valence to the conduction band.

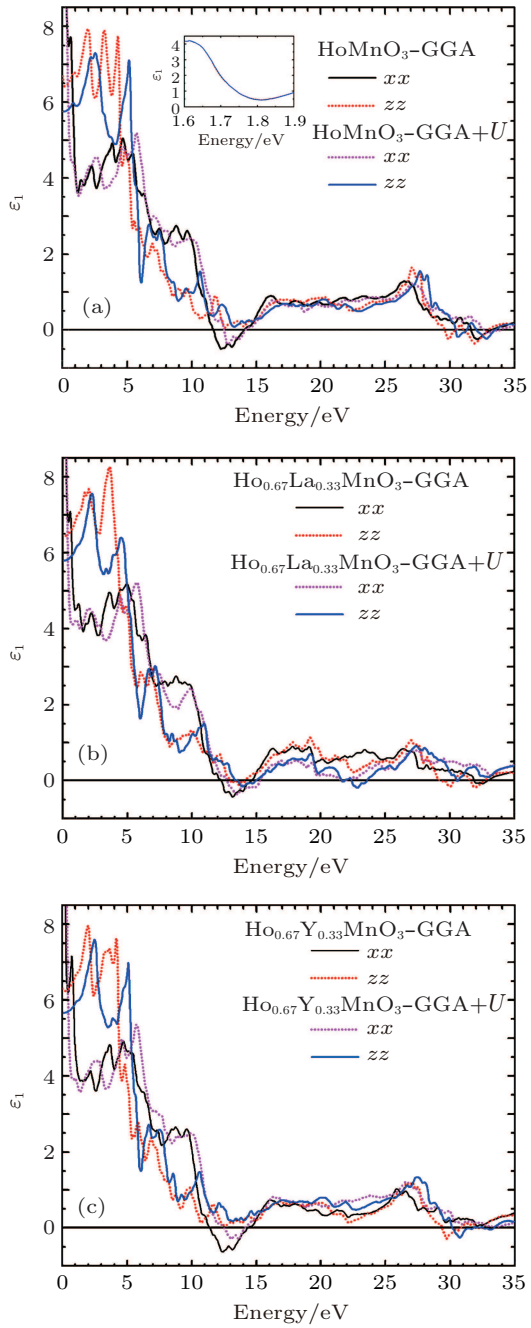


Fig. 6. (color online) Real parts of dielectric function for $Ho_{1-x}T_xMnO_3$: (a) $x = 0$; (b) $x = 0.33$, T = La; (c) $x = 0.33$, T = Y. The inset is cited from Ref. [4].

Pure $HoMnO_3$, as can be seen from the DOS plots, is predicted to behave as a metal along the x direction within the SPGGA calculations. In the x direction, E_0 and E_2 are related to the transitions from the occupied Mn-3d states at -0.79 eV to the unoccupied ones at 1.05 eV. The E_3 is the transition from the top of the valence band to the bottom of the conduction band. On the other hand, for the z direction, E_0 is related to the transition from the occupied to unoccupied Ho-4f states situated on the Fermi level. The E_1 is the transition from the top of the VB (occupied Ho-4f around -0.85 eV) to the unoccupied Ho-4f states (around 0.12 eV). The E_2 and E_3 are the transitions from the occupied Ho-4f states (around -0.85 eV) to the unoccupied Mn-3d states around 1.70 eV and 2.82 eV, respectively.

The metallic behavior is also predicted for pure $HoMnO_3$ by means of SPGGA + U. In this approximation, E_0 is the transition from the occupied to the unoccupied Mn-3d state around the Fermi level. Also E_1 is the transition from the top of the VB to the bottom of the CB. The E_2 and E_3 are the transitions from the occupied Mn-3d or O-2p (around -1.93 eV) and Ho-4f (around -3.60 eV) states to the unoccupied Mn-3d states around 1.63 eV, respectively. However, for the z direction, E_0 is the transition from the top of the VB to the bottom of the CB, E_1 is the transition from the occupied Ho-4f (at -0.60 eV) to the unoccupied ones (at 1.22 eV), E_2 is the transition from the occupied Ho-4f state (at -0.60 eV) to the unoccupied Mn-3d state in the CB (around 2.31 eV), and E_3 is the transition from O-2p (at -2.41 eV) to the unoccupied Ho-4f state (at 1.12 eV).

Nevertheless, in all studied materials, we can see a tangible shift toward higher energies when the used approximation changes from SPGGA to SPGGA + U, which is more noticeable and obvious along the z direction. The results show that substitution of La and Y for Ho_1 in $HoMnO_3$ causes the imaginary part of the dielectric function to move toward lower energies, which is more striking for $Ho_{0.67}La_{0.33}MnO_3$ along the z direction than for $Ho_{0.67}Y_{0.33}MnO_3$.

6. Optical conductivity

We use the following relation to calculate the real part of the optical conductivity:

$$\mathrm{Re}\sigma_{\alpha\beta}(\omega) = \frac{\omega}{4\pi}\mathrm{Im}\varepsilon_{\alpha\beta}(\omega). \tag{3}$$

The real parts of the optical conductivity spectra for all studied materials are shown in Fig. 8. These spectra show peaks due to the transition from VB to CB. We can see from the data that the early four peaks ($E_1 = 1.15$, $E_2 = 2.27$, $E_3 = 3.66$, and $E_4 = 4.42$) along the z direction (in the SPGGA approximation) for pure $HoMnO_3$ are in relatively good agreement with the experimental data at 6 K cited from Ref. [4]. The maximum optical conductivity 7.4×10^{15} s^{-1} is observed around 28 eV (for the z direction) and also a smaller conductivity peak 5.5×10^{15} s^{-1} exists around 10 eV (for the x direction) for $HoMnO_3$ within the SPGGA calculations. The results show that by substituting La and Y for Ho_1 in the pure compound, the maximum optical conductivity decreases in the z direction.

7. Conclusion

The structural, optoelectronic, and magnetic properties of $Ho_{1-x}T_xMnO_3$ ($x = 0$, 0.33; T = La, Y) are investigated by the density functional theory within the SPGGA and SPGGA + U approximations. For both approximations, the band gap increases by doping La and Y atoms to the pure $HoMnO_3$ in the spin-up state. Our results predicate that the substitutions of

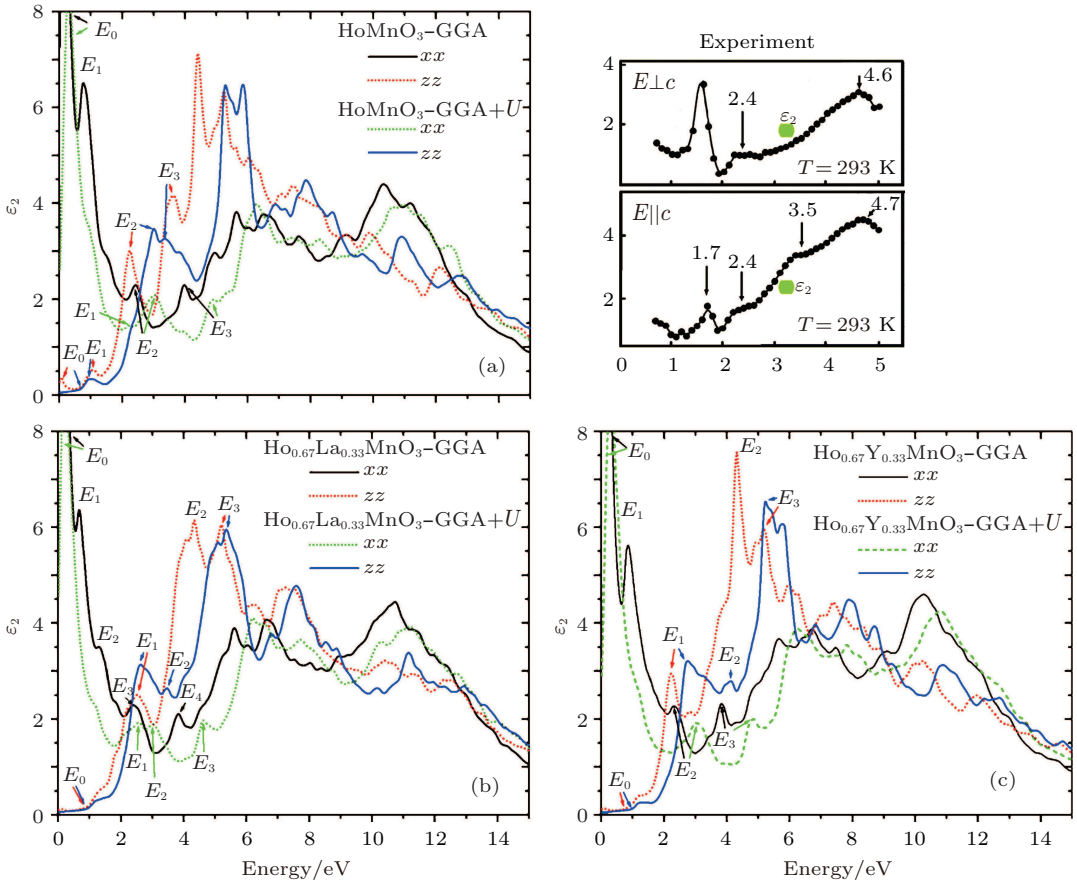


Fig. 7. (color online) Imaginary parts of dielectric function for $Ho_{1-x}T_xMnO_3$: (a) $x = 0$; (b) $x = 0.33$, T = La; (c) $x = 0.33$, T = Y. The experimental curves are cited from Ref. [2].

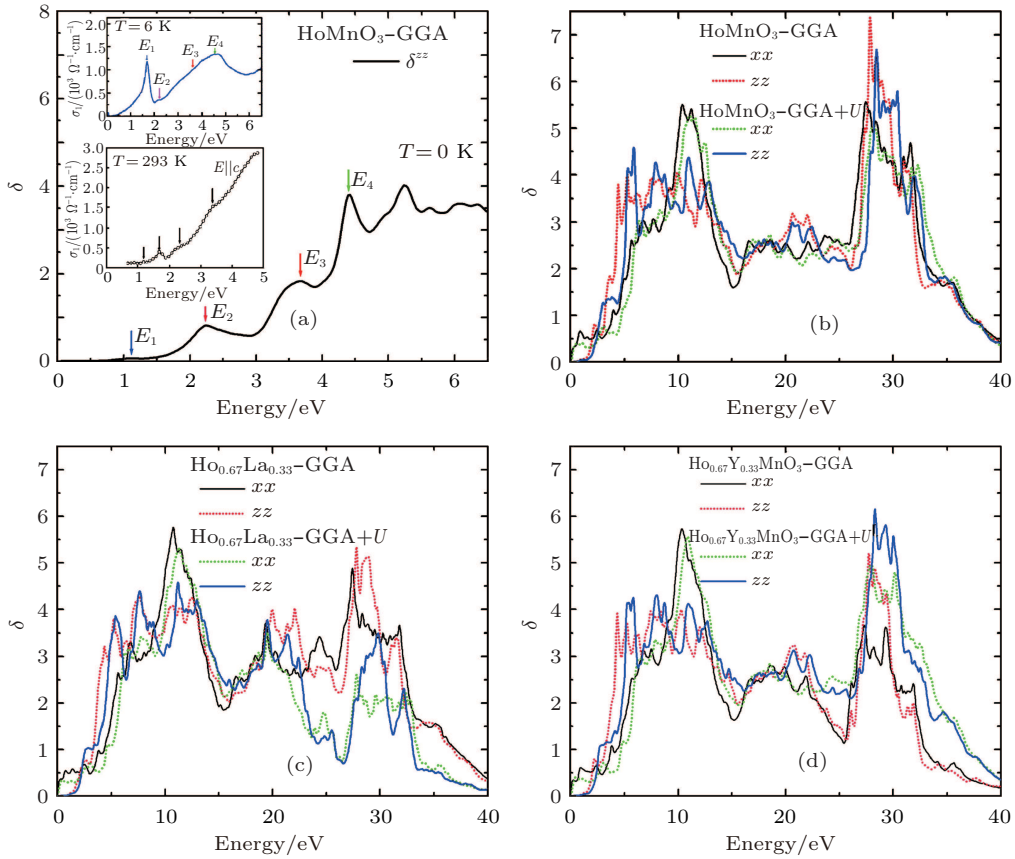


Fig. 8. (color online) Real parts of optical conductivity ($\times 10^{15}$ s^{-1}) for $Ho_{1-x}T_xMnO_3$: (a), (b) $x = 0$; (c) $x = 0.33$, T = La; (d) $x = 0.33$, T = Y. The insets are cited from Ref. [4].

La and Y atoms for Ho_1 change the c parameter and the magnetic properties. The net magnetic moment of $HoMnO_3$ originates from the contribution of the magnetic moments of the unfilled Ho_1-4f, Ho_2-4f, Mn-3d states and the interstitial sites. The results show that the magnetic moment at the Mn site increases by adding La and Y atoms. For the optical properties, the metallic behavior is predicted for pure $HoMnO_3$. By substituting La and Y for Ho_1 in pure $HoMnO_3$, the maximum optical conductivity decreases in the z direction. The obtained optical spectra are in close agreement with the experimental results.

Acknowledgment

The authors are grateful to P. Blaha (Vienna University of Technology, Austria) for his technical assistance in using the WIEN2k code.

References

[1] Lonkai Th, Hohlwein D, Ihringer J and Prandl W 2002 *Appl. Phys. A* **74** 843
[2] Makhneva A A, Nomerovannayaa L V and Balbashovb A M 2011 *Physics of the Solid State* **53** 105
[3] Ederer C and Spaldin N A 2005 *Current Opinion in Solid State and Materials Science* **9** 128
[4] Rai R C, Cao J, J L Musfeldt, Kim S B, Cheong S W and Wei X 2007 *Phys. Rev. B* **75** 184414
[5] Dela Cruz C, Yen F, Lorenz B, Wang Y Q, Sun Y Y, Gospodinov M M and Chu C W 2005 *Phys. Rev. B* **71** 60407
[6] Gao P, Chen Z, Tyson T A, Wu T, Ahn K H, Liu Z, Tappero R, Kim S B and Cheong S W 2011 *Phys. Rev. B* **83** 224113
[7] Gibbs A S, Knight K S and Lightfoot P 2011 *Phys. Rev. B* **83** 094111
[8] Lottermoser T, Lonkai T, Amann U, Hohlwein D, Ihringer J and Fiebig M 2004 *Nature* **430** 541
[9] Nandi S, Kreyssig A, Tan L, Kim J W, Yan J Q, Lang J C, Haskel D, McQueeney R J and Goldman A I 2008 *Phys. Rev. Lett.* **100** 217201
[10] Murugavel P, Lee J H, Lee D, Nohb T W, Younghun J, Myung-Hwa J, Seok O Y and Hoon K K 2007 *Appl. Phys. Lett.* **90** 142902
[11] Blaha P, Schwarz K, Madsen G, Kvasnicka D and Luitz J 2011 *WIEN2k User's Guide* (Vienna University of Technology in Austria)
[12] Perdew P J, Burke K and Ernzerhof M 1996 *Phys. Rev. Lett.* **77** 3865
[13] Anisimov V I, Solovyev V I, Korotin M A, Czyżyk M T and Sawatzky G A 1993 *Phys. Rev. B* **48** 16929
[14] Petukhov A G and Mazin I I 2003 *Phys. Rev. B* **67** 153106
[15] Novák P, Kuneš J, Chaput L and Pickett W E 2006 *Phys. Status Solidi B* **243** 563
[16] Madsen G K H and Novák P 2005 *Europhys. Lett.* **69** 777
[17] Erhart P, Klein A, Egdell R G and Albel K 2007 *Phys. Rev. B* **75** 153205
[18] Chong G Z, Jing H F, Jian H Y, Zheng C D and Xue F J 2011 *Acta Phys. Chim. Sin.* **27** 388
[19] Choi W S, Kim D G, Seo S S A, Moon S J, Lee D, Lee J H, Lee H S, Cho D Y, Lee Y S, Murugavel P, Yu J and Noh T W 2008 *Phys. Rev. B* **77** 045137
[20] Bertaut E F and Mercier M 1963 *Phys. Lett.* **5** 27
[21] Vajk O P, Kenzelmann M, Lynn J W, Kim S B and Cheong S W 2005 *Phys. Rev. Lett.* **94** 087601
[22] Condran S G and Plumer M L 2010 *J. Phys.: Condens. Matter* **22** 16220
[23] Rahnamaye Aliabad H A and Ahmad I 2012 *Physica B* **407** 368
[24] Wooten F 1972 *Optical Properties of Solids* (New York: Academic Press) pp. 114–115